Available online at www.sciencedirect.com
ScienceDirect
European Journal of Mechanics B/Fluids 25 (2006) 554–564

Experimental velocities and accelerations in very steep wave events in deep water

John Grue *, Atle Jensen

Mechanics Division, Department of Mathematics, University of Oslo, Norway

Received 22 December 2005; received in revised form 27 March 2006; accepted 27 March 2006

Available online 5 June 2006

Abstract

The entire experimental velocity and acceleration fields in the six steepest cases of a campaign of totally 122 large wave events in deep water are documented. From observations in these six waves, totally 36000 experimental velocity vectors are put on non-dimensional form using a suitable reference velocity defined by $\epsilon\sqrt{g/k}$, where k and ϵ are obtained as follows: from the wave record at a fixed position the local trough-to-trough period, $T_{\rm TT}$ and the maximal elevation of the event above mean sea level, ζ_m are defined. The local wavenumber, k and the wave slope, ϵ are evaluated from $\omega^2/(gk) = 1 + \epsilon^2$ and $k\zeta_m = \epsilon + \frac{1}{2}\epsilon^2 + \frac{1}{2}\epsilon^3$ where $\omega = 2\pi/T_{\rm TT}$ and $g = 9.81$ m/s^2. The wave slope for the large wave events in laboratory shown here is in the range 0.40–0.46 and is realized for focussing wave events. The procedure employed to measurements in the field estimates $\epsilon \simeq 0.39$ for the Draupner wave and $\epsilon \simeq 0.38$ for the Camille wave. The horizontal velocities obtained in the laboratory campaign are always less than the wave speed. The velocity vector has magnitude comparable to the wave speed in the strongest case and is manifested in the jet that develops at the front face of the breaking waves. The non-breaking waves exhibit a maximal horizontal acceleration up to about $0.7g$ in the front face of the wave at vertical level about half way to the crest. The overturning events exhibit horizontal accelerations up to $1.1g$ and vertical accelerations up to $1.5g$ in the front face of the wave, at the base below the overturning jet. The wave profile and the velocity and acceleration fields exhibit strong front/back asymmetry. The acceleration vectors extracted in close vicinity of the wave contour plus the acceleration of gravity along the (positive) vertical give vectors that are close to the normal of the surface contour.

Keywords: Draupner wave; Camille wave; Rogue waves; Velocities; Accelerations; PIV; Experimental freak waves; Velocity scale

1. Introduction

Current research on very large waves at sea is pursued mainly along the theoretical and numerical direction. The main goal is to understand and predict the most important mechanisms leading to the organization and the build-up of the very large waves that can be documented, such as the Draupner and Camille waves. The observations and measurements of the very large waves in the field and in the laboratory represent a compliment to the theoretical development, however. The present experimental study is prepared in response to the request for up-to-date and reliable observational and experimental data of rogue waves.

* Corresponding author.
E-mail address: johng@math.uio.no (J. Grue).

0997-7546/$ – see front matter
doi:10.1016/j.euromechflu.2006.03.006

We report here the velocity and acceleration fields in six very large wave events that were realized in a series of wave tank experiments. The wave slope is in the range 0.40–0.46 and exceeds previously published laboratory studies of large waves Kim et al. [1], Baldock et al. [2], Skyner [3] by a factor of about 50%. The wave events are deep water waves with kh in the range 3.6–5.0, where k denotes the wavenumber and h the water depth, and are the largest samples that were measured in an extensive experimental campaign measuring 122 large wave events. While the velocity and acceleration fields of the waves are published here for the first time, the velocity profile below crest of the 122 large wave events were presented on a dimensionless form using the scaling (1) below that was introduced in Grue et al. [4]. The velocity and acceleration fields are presented in hodograph (vector) plots in non-dimensional form.

Measurements of the surface elevation obtained by resistance wave gauges are combined with Particle Image Velocimetry (PIV) of the velocities and accelerations below the waves. The latter are obtained in sections about one quarter wave length long and deep below the crest. The velocity measurements are related to previous studies by Kim et al. [1], Baldock et al. [2] using Laser Doppler Anemometry and by Skyner [3] using PIV. All the three studies have a common maximal wave slope in the range 0.28–0.30 but differ fundamentally with respect to the effect of a finite water depth. In the work by Baldock et al. [2] the non-dimensional water depth was $kh = 3.2$ and the measured maximal fluid velocity 40% of the estimated wave speed. The same parameters were 2.0 and 64% in Kim et al. [1] and 2.6 and 114% in Skyner [3], respectively. (We have recomputed the values of the wave slope and wavenumber from the time series given in Kim et al. [1] and Baldock et al. [2] using the scaling (1) below.) Such high relative velocities have neither been observed by Baldock et al. [2] nor in the present campaign with large kh, for wave slopes around $\epsilon \sim 0.3$. The velocity measurements by Kim et al. [1] and Skyner [3] do not exhibit the same collapse of the non-dimensional data as presented here (see below). (In an experimental campaign Perlin et al. [5] they measured velocities up to 130% of the phase speed of the (equivalent) linear wave. An estimate of the wave slope ϵ is not available.)

For the velocity fields we shall use the scaling introduced and justified by Grue et al. [4], finding a collapse of the measured velocity profiles below crest. The appropriate velocity scale is obtained by first defining a wave slope, ϵ and a wavenumber, k of the individual large wave event. A reference velocity is then defined by $u_{\mathrm{ref}} = \epsilon\sqrt{g/k}$, and non-dimensional velocity vectors by $(\hat{u}, \hat{v}) = (u, v)/u_{\mathrm{ref}}$. The ϵ and k are obtained from the time record of the surface elevation where the maximal elevation, ζ_m and trough-to-trough period of the event, T_{TT} are determined. We then define $\omega = 2\pi/T_{\mathrm{TT}}$ and compute ϵ and k from

$$\frac{\omega^2}{gk} = 1 + \epsilon^2, \qquad k\zeta_m = \epsilon + \frac{1}{2}\epsilon^2 + \frac{1}{2}\epsilon^3. \tag{1}$$

By this procedure the velocities are presented on a non-dimensional form, with a rather strong collapse of the (dimensional) velocity data as result Grue et al. [4]. We have tested the procedure in fully nonlinear simulations comparing the actual wave length with the estimated one ($= 2\pi/k$), finding a relative difference of 3.5% for $k\zeta_m = 0.34$. In the campaign Grue et al. [4] we played a little with the choice of the local wave period, finding that the trough-to-trough and zero down-crossing periods gave about the same results, but that the zero up-crossing period gave significant spread in the non-dimensional velocity plots. We note that the trough-to-trough period (and wave length) is a much used reference in experimental papers dealing with highly nonlinear wave phenomena Su [6].

Focussing waves were generated in the 24.6 m long wave tank in the Hydrodynamic Laboratory at the University of Oslo. The tank width is 0.5 m and the water depth 0.72 m. Further specification of the wave generation procedure and other relevant experimental parameters are given in Grue et al. [4, §4.2]. The velocities and the material acceleration fields of the waves is obtained by employing an extended PIV system Jensen et al. [7]. The system, particularly designed to measure accelerations, consists of two CCD cameras and a CW argon ion laser together with a scanning beam system. Polyamid particles with diameter 50 μm were used for seeding. The velocity and material acceleration fields of the waves in vicinity of the crest were obtained by the procedure and optimization technique documented in Jensen and Pedersen [8] and Jensen et al. [9].

The wave elevation at the measurement position (of the PIV equipment) of the six experiments in focus are plotted in Fig. 1. The first (and steepest) event in each of the runs is studied.

The six events are divided into two groups. The first three waves are non-breaking events with estimated wave slope ϵ that equals 0.4 (case A), 0.44 (case B) and 0.45 (case C). These waves may later develop breaking. The remaining three waves exhibit a beginning overturning in the top part of the waves and have estimated wave slope 0.41 (case D),

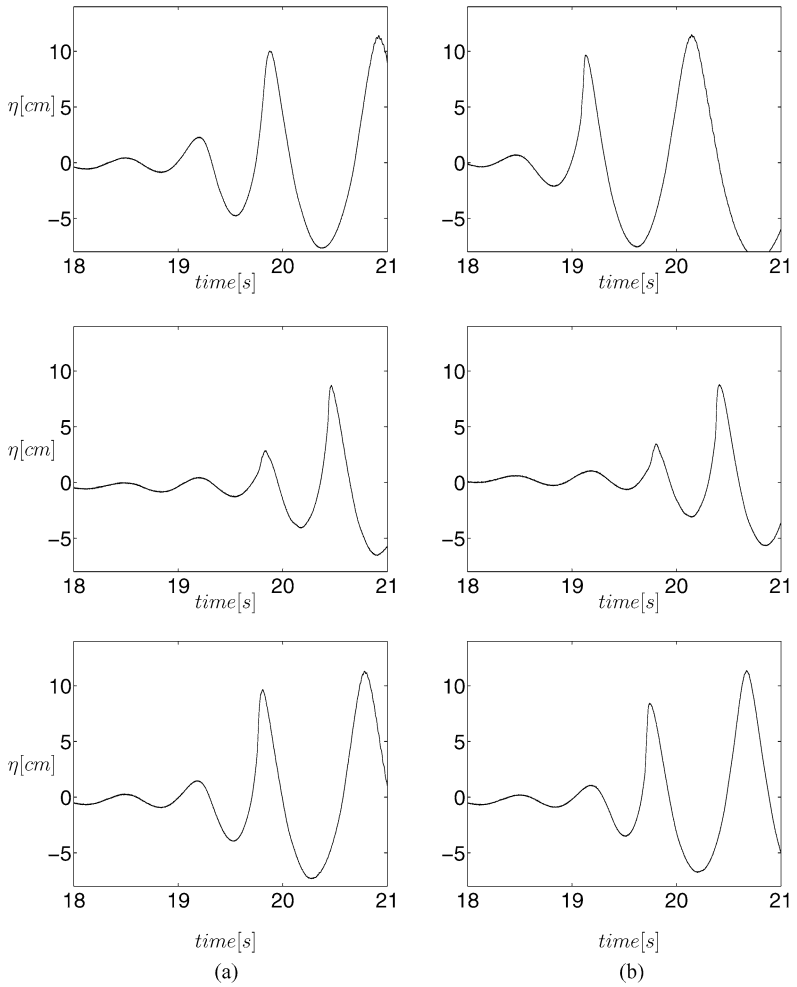

Fig. 1. The six steepest events $0.4 < \epsilon < 0.46$. (a) From top: case A, B, C. (b) From top: case D, E, F.

0.44 (case E) and 0.46 (case F). The latter is the largest we have studied in the wave tank. Images of the waves and the velocity arrows from PIV are presented in Fig. 12 and the accelerations in Fig. 13.

The recorded velocity profile below crest, more precisely at the position of the vanishing vertical velocity – extracted from the maps of the velocity fields, is plotted in Fig. 2 for the six events. The measured velocities exhibit a good collapse when presented on the non-dimensional form using the procedure indicated above. The LDA measurements from Baldock et al. [2] – with quite different ϵ of the wave – is replotted on non-dimensional form in the figure, finding agreement with the present measurements. We have also included the velocity profile below crest of the steepest wave event modelled by Clamond and Grue [10] (their and Fig. 1), showing the same non-dimensional behaviour as in the measurements. The exponential profile, $\exp(ky)$ is plotted in the figure for reference as well (which gives the velocity profile in the case of a Stokes wave in deep water). The usefulness of the reference velocity u_{ref} with (1) is indicated by the collapse of the data presented in Fig. 2.

1.1. Estimates of ϵ for the Draupner and Camille waves

The measurements of the laboratory waves may be put into perspective by evaluating the wavenumber and wave slope of large waves that have been observed at sea, such as the Draupner wave and the Camille wave. The time series of the Draupner wave is provided in e.g. Fig. 1 in Trulsen [11], see also Fig. 1 in Walker et al. [12]. From the time series of the surface elevation the trough-to-trough period and the maximal elevation above mean sea level are

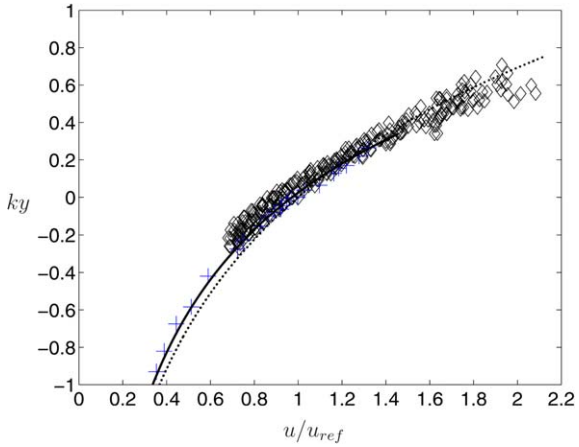

Fig. 2. $\diamond\diamond\diamond$ non-dimensional velocity profile below crest of all the six large wave events, $+++$: LDA-measurements by Baldock et al. [2] (with $\epsilon = 0.29$). $-$ Fully nonlinear computations by Clamond and Grue [10], $\cdots$: $\exp(ky)$.

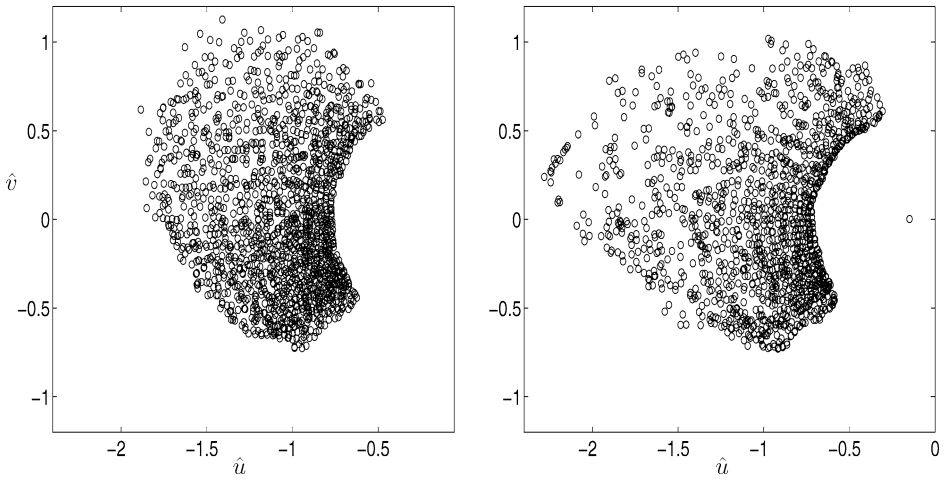

Fig. 3. Velocity plane plots of vectors $(\hat{u}, \hat{v}) = (u, v)/u_{\text{ref}}$. From left: case A and B.

estimated to: $T_{\text{TT}} = 11.5$ s and $\zeta_m = 18.5$ m, respectively. The value of $(2\pi/T_{\text{TT}})^2\zeta_m/g$ becomes 0.563. Putting the quantities into Eqs. (1) we obtain $k\zeta_m \simeq 0.49$ and $\epsilon \simeq 0.39$ for the Draupner wave.

The time series of the Camille wave is given in Fig. 8.1 (p. 218) in Ochi's book Ochi [13]. From the time series that is a reproduction of the wave in laboratory we estimate the trough-to-trough period to 0.72 s, the wave height to $H = 10.3$ cm and the maximal elevation above mean sea level to $\zeta_m = 7.2$ cm. The value of $(2\pi/T_{\text{TT}})^2\zeta_m/g$ becomes 0.559. Putting these quantities into Eqs. (1) we obtain

$$k\zeta_m \simeq 0.49 \quad \text{and} \quad \epsilon \simeq 0.38$$

for the Camille wave. (Estimates based on the given wave height H gives $kH \simeq 0.72$ and $\epsilon \simeq 0.34$.)

2. Velocity measurements

Figs. 3–5 show the (non-dimensional) velocity vector plots due to all the six waves. For reference of the non-dimensional values, we estimate the wave propagation speed by evaluating ω/k. In non-dimensional terms the value of $[\omega/k]/u_{\text{ref}}$ is estimated by $\sqrt{1+\epsilon^2}/\epsilon$, see Eq. (1), giving a non-dimensional propagation speed of 2.7 (case A), 2.6 (case D), 2.5 (cases B and E), and 2.4 (cases C and F).

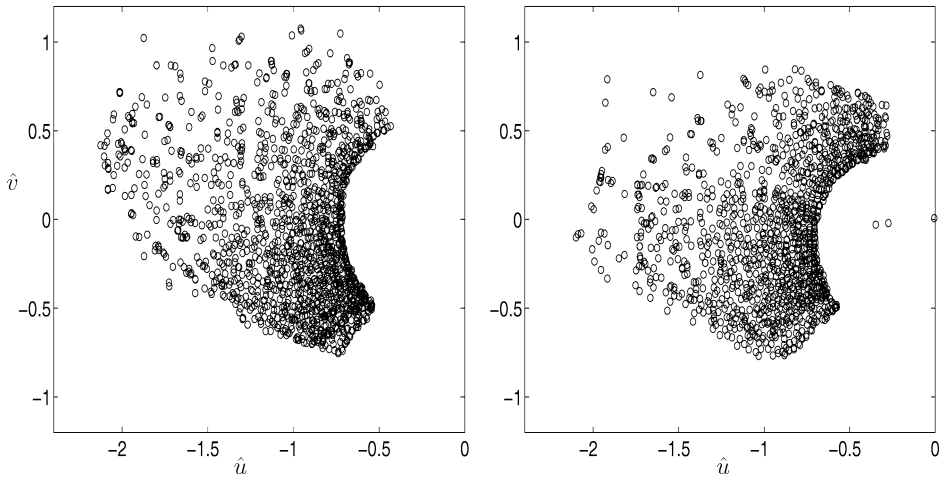

Fig. 4. Same as previous figure, but case C (left) and D (right).

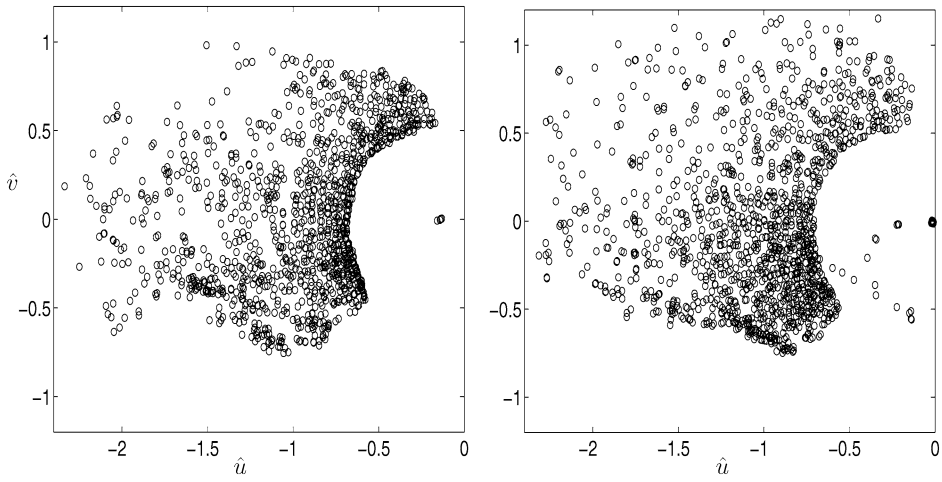

Fig. 5. Same as previous figure, but case E (left) and F (right).

All together 36000 velocity vectors are plotted in the figures. The horizontal velocity is always negative since the waves are moving from right to left in the experiments. We note that the contour that follows the smallest velocity vectors – the velocity vectors observed for the lowest vertical coordinate – is relatively close to a circle in all cases. The velocity fields are asymmetric in the sense that velocities generally are larger in front part of the wave than in the back. This asymmetry is increasing with nonlinearity and with the level of the vertical coordinate.

The plots show that the horizontal velocity can expect a maximum where the vertical velocity is slightly positive. This occurs at a small distance ahead of the position where $hv = 0$. This distance is slightly growing with the wave slope for the non-breaking cases B and C. Maximal horizontal velocities are observed all along the top part of the wave for the overturning cases D–F.

The horizontal velocity component has a maximal non-dimensional value of 2.3 in all experiments and is always smaller than the estimated wave propagation speed. The absolute value of the velocity vector $\sqrt{\hat{u}^2 + \hat{v}^2}$ has a maximal value of 2.4 in the front part – the tip – of the wave in case F. This corresponds to the magnitude of the wave propagation velocity. The velocity vector is always less than the wave speed in all cases other than F, however.

We are using the grid size $N = 32$ with 50% overlap in the PIV algorithm and we are able to get reliable vectors the distance $N/2$ from the free surface. The field of view (FOV) is 25×20 cm and the resolution of the cameras are 1280×1024 pixels. The distance to the first velocity vector is 0.3125 cm.

3. Acceleration measurements

Very few acceleration measurements below steep waves exist. In the experimental study by Kim et al. [1] using LDA they estimated a maximal downward vertical acceleration of $-0.47g$ and a horizontal acceleration of $0.39g$ (their wave was moving from left to right). The accelerations in the breaking tip of a wave that was generated by an impulsive piston motion were measured in a distance of 0.35 m from the wave paddle to be $1.1g$ by Chang and Liu [14] using PIV. These measurement fit into the ensemble of acceleration measurements that are presented in Figs. 6–11.

We plot here acceleration vectors that are scaled by the acceleration of gravity (g). The material (full) acceleration vector is obtained, including the local and the convective terms. Three types of acceleration plots are given: first we show the vertical component of the acceleration vector as a function of the vertical coordinate, next the horizontal component versus the vertical coordinate is plotted, and finally the acceleration vector field is plotted in the acceleration vector plane. The plots are grouped into the non-breaking cases A–C and the breaking cases D–F.

First we note that in the case of Stokes waves, the length of the horizontal acceleration vector divided by g is indicated by the wave slope. In our case the wave slope is in the range 0.4–0.46 which indicates the expected level of the non-dimensional accelerations. This level is confirmed for the vertical accelerations that are presented for cases A–C in Fig. 6. Indeed, the maximal negative acceleration has a non-dimensional value of (about) 0.45 corresponding to the value of ϵ in case C. This value would also have given the maximal positive acceleration, had we presented measurements for the entire wave cycle, which we did not intend to do, however. Instead, the results in Fig. 6 exhibit a positive vertical acceleration up to about $0.6g$ at a vertical level of the wave between 2 and 6 cm above mean water level in the laboratory coordinate system. This is about half-way to the level of the crest, and are acceleration vectors in the front part of the wave. We note that this rise in the vertical acceleration is not seen in the smoothest wave (still steep) in the case A.

The horizontal component of the acceleration field in the front part of the wave exhibits the same level as the vertical one. This level of the accelerations is a feature of the region between 2 and 6 cm above mean water level, in the front part of the wave (Fig. 7). The number of acceleration vectors with a high negative horizontal component in the front part of the wave – along the propagation direction – is significantly higher than vectors which are high in both directions. This is also confirmed in the hodograph plot in Fig. 10 which shows a_y/g vs. a_x/g: the vast majority of the acceleration vectors with a_x/g around -0.6 has negative vertical acceleration a_y/g in the range between -0.4 and -0.1, and only a few vectors with $a_x/g \sim -0.6$ and a_y/g in the range between 0 and 0.6. These accelerations are observed in a thin region along the upward moving free surface in the front part of the wave, at a vertical level corresponding to half the crest height.

The same tendencies of the accelerations are observed for the stronger cases D–F: The maximal negative non-dimensional vertical acceleration below crest has a value corresponding to the wave slope (Fig. 8). The vertical accelerations in the front part of the waves have now increased to a maximal level of g (several vectors) with a few vectors exceeding g by 50%. The extreme acceleration vectors are few and occur in a very limited region in the front part of the wave at a vertical level that is midway to the crest.

The same increase is observed in the horizontal accelerations in front part of the wave. A very systematic negative horizontal acceleration that somewhat exceeds g – directed along the propagation – occurs in the front part of the wave midway to the crest level (Fig. 9). The figure exhibits some outliers without reasonable physical explanation.

The acceleration vector plot for cases D–F shows a strong increase in the acceleration vectors that have a large negative horizontal component as well as a large vertical component (Fig. 11). The maximal negative horizontal acceleration is around $-1.1g$, while the upward vertical acceleration component systematically grows beyond g and reaches a maximal value of about $1.5g$ in the present examples. This corresponds to an acceleration vector with length

$$\sqrt{a_x^2 + a_y^2} \sim 1.9g$$

taking part in the front part of the wave at vertical level midways to the crest.

Finally we note that the vector difference between the particle acceleration and the acceleration of gravity determines the pressure gradient. The latter is normal to the zero pressure contour separating the water and air phases – easily determined from the images. The acceleration vectors that are obtained in the front part of the wave using the PIV method plus g along the (positive) vertical are indeed (close to) normal to the wave contour, see the acceleration plots in Fig. 13.

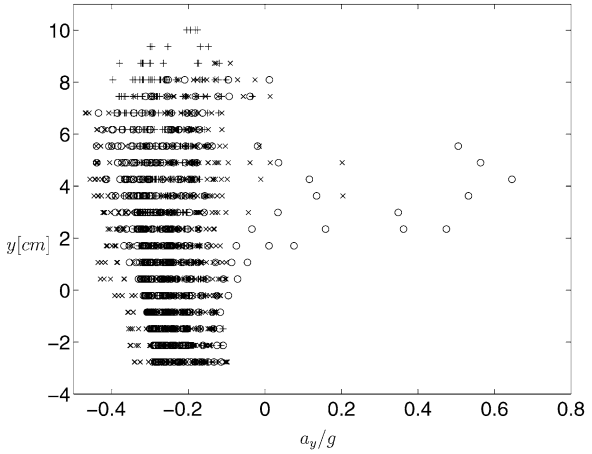

Fig. 6. Vertical acceleration a_y/g vs. vertical position y in waves, cases A(+), B(x), C(o).

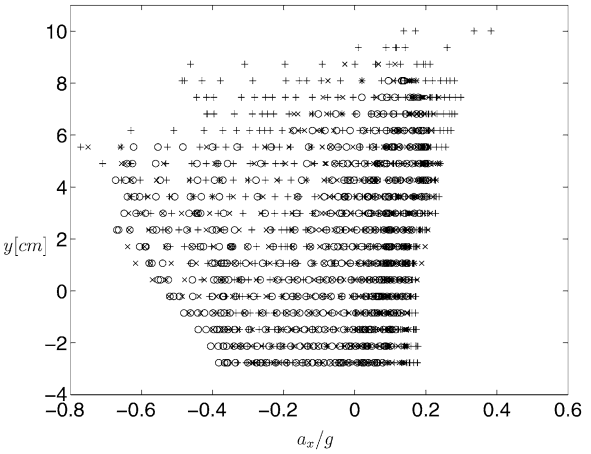

Fig. 7. Horizontal acceleration a_x/g vs. vertical position y in waves, cases A(+), B(x), C(o).

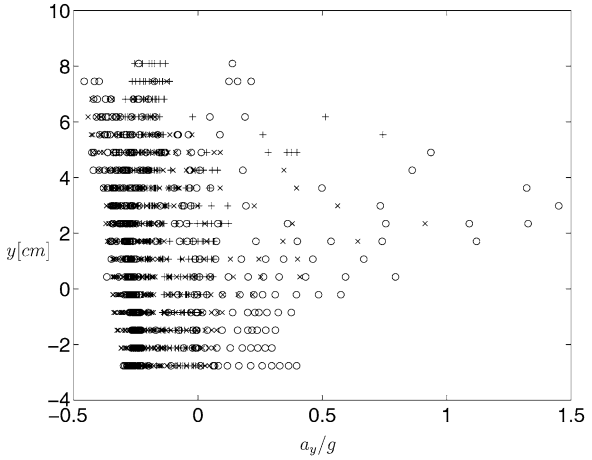

Fig. 8. Vertical acceleration a_y/g vs. vertical position y in waves, cases D(+), E(x), F(o).

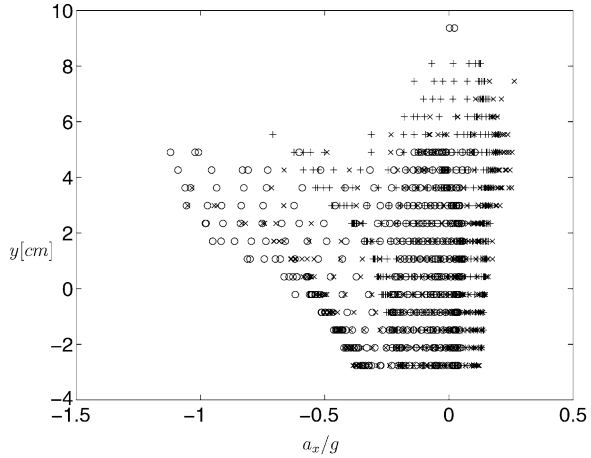

Fig. 9. Horizontal acceleration a_x/g vs. vertical position y in waves, cases D(+), E(x), F(o).

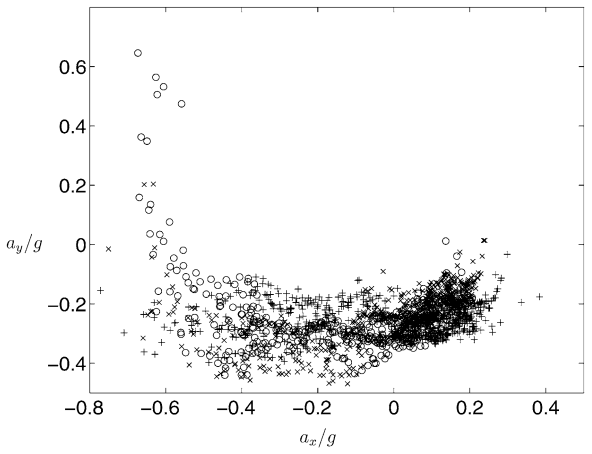

Fig. 10. Acceleration plane plot of all velocity vectors in waves, cases A, B, C.

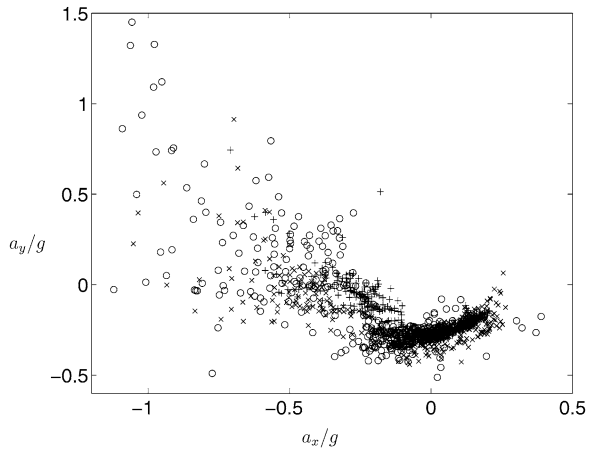

Fig. 11. Acceleration plane plot of all velocity vectors in waves, cases D, E, F.

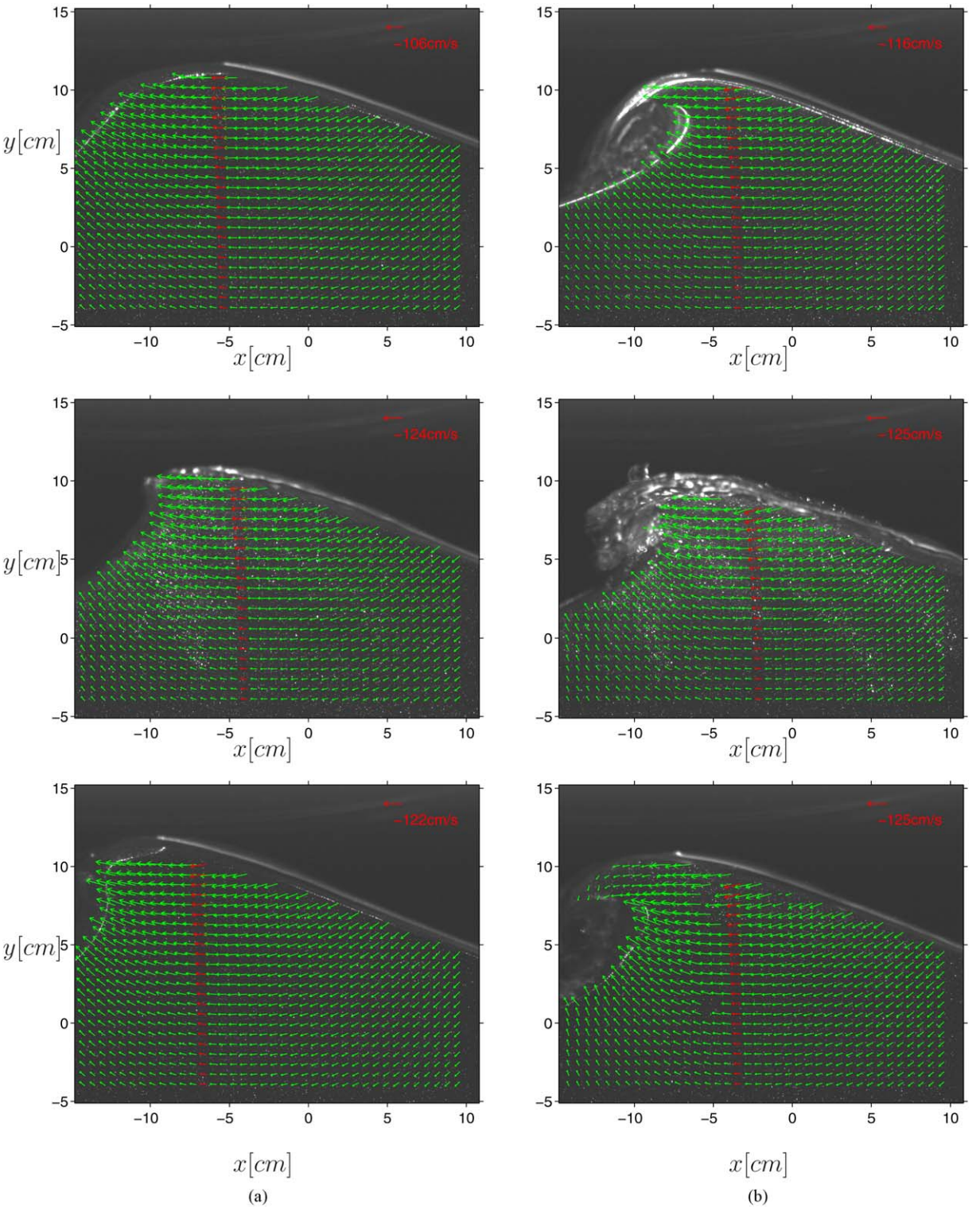

Fig. 12. Velocity field on top of bitmap from PIV recording. (a) From top: case A, B, C. (b) From top: case D, E, F. Case A: $\epsilon = 0.40$, $k\eta_m = 0.51$, $kh = 3.6$. Case B: $\epsilon = 0.44$, $k\eta_m = 0.58$, $kh = 4.6$. Case C: $\epsilon = 0.45$, $k\eta_m = 0.60$, $kh = 4.3$. Case D: $\epsilon = 0.41$, $k\eta_m = 0.53$, $kh = 3.9$. Case E: $\epsilon = 0.44$, $k\eta_m = 0.58$, $kh = 4.8$. Case F: $\epsilon = 0.46$, $k\eta_m = 0.62$, $kh = 5.0$.

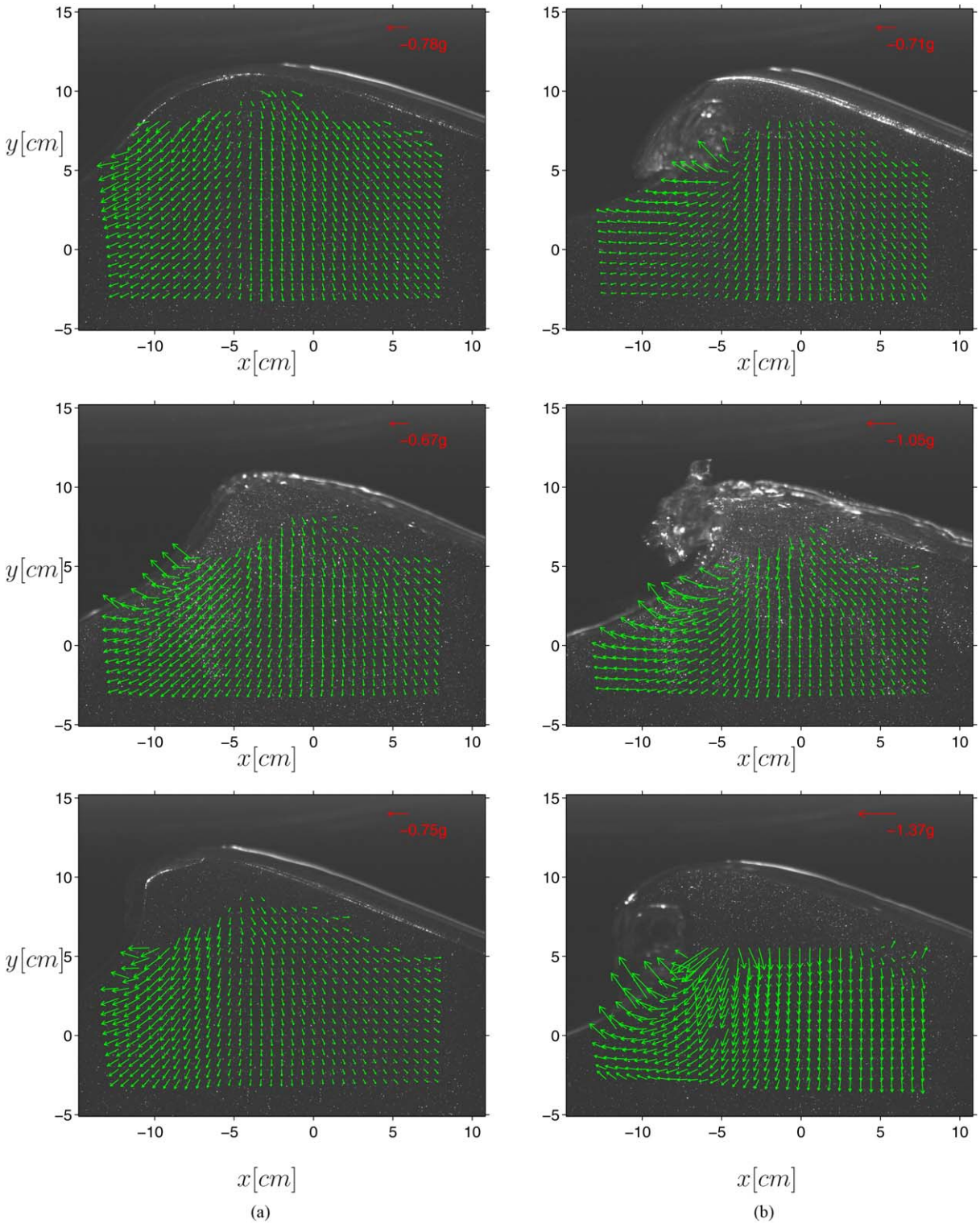

Fig. 13. Acceleration field on top of bitmap from PIV recording. (a) From top: case A, B, C. (b) From top: case D, E, F. Case A: $\epsilon = 0.40$, $k\eta_m = 0.51$, $kh = 3.6$. Case B: $\epsilon = 0.44$, $k\eta_m = 0.58$, $kh = 4.6$. Case C: $\epsilon = 0.45$, $k\eta_m = 0.60$, $kh = 4.3$. Case D: $\epsilon = 0.41$, $k\eta_m = 0.53$, $kh = 3.9$. Case E: $\epsilon = 0.44$, $k\eta_m = 0.58$, $kh = 4.8$. Case F: $\epsilon = 0.46$, $k\eta_m = 0.62$, $kh = 5.0$.

4. Conclusion

In summary, the velocity fields below crest of six very steep wave events in deep water with an estimated wave slope in the range 0.40–0.46 exhibit horizontal velocities that are always less than the (estimated) wave speed. A maximal horizontal velocity is observed somewhat ahead of the wave crest. The large unstable waves develop overturning, and velocities in three strong waves were measured in this phase. The horizontal velocity is found to have approximately the same magnitude over a small horizontal distance in the top part of the wave. In the strongest case observed here the magnitude of the velocity vector in the jet of the wave becomes comparable to the estimated wave speed. The strong waves become strongly asymmetric.

The magnitude of the wave induced accelerations at some distance from the front face of the waves can be inferred from steady waves, namely the wave slope times g. In the present examples the wave slope is in the range 0.40–0.46, and so is the range of the non-dimensional accelerations in the vast part of the wave field. The measurements show larger accelerations in the front face of the wave, however. We have in particular investigated three non-breaking cases (the unstable waves break further down-stream) where the level of the horizontal acceleration is up to $0.7g$ directed along the wave propagation. This horizontal acceleration appears in a very systematic way and with many occurrences in the acceleration vector plot. A similar vertical acceleration is induced in the front face of the wave, but is observed for fewer acceleration vectors. These high accelerations take place in the front face of the wave at a vertical level about half way to the crest.

The group of waves with a developing overturning jet exhibit accelerations in the base below the jet that are up to $1.1g$ along the horizontal direction and up to $1.5g$ along the vertical. Again, the large horizontal acceleration is observed in significantly more points than the large vertical acceleration.

The results here should be compared to the computations of overturning waves in water of finite (moderate) depth New et al. [15], Dommermuth et al. [16] which exhibits velocities in the overturning jet up to 1.5 times the phase velocity and very large accelerations on – and in the near vicinity of – the strongly curved surface below the jet. Maximal values of the acceleration up to $6g$ were calculated in the horizontal and vertical directions. The overturning process in steep waves has also been simulated using a 2D Navier–Stokes solver (Volume of Fluid Method) where the effect of surface tension is included Chen et al. [17]. The velocity and acceleration fields prior to breaking exhibited very large velocities particularly in the plunging jet. These exceeded the estimated phase speed by about 76% in the strongest case. Accelerations up to $3.5g$ were computed below the jet.

The acceleration vectors that are extracted in the close vicinity of the wave contour plus the acceleration of gravity g along the (positive) vertical give vectors that are (close to) normal to the wave contour, see the acceleration plots in Fig. 13. We note that it is more difficult to acquire accelerations than velocities. The pseudo tracking technique used herein needs several velocity vectors to have a reliable material acceleration. The group of particles close to the free surface is moving with very large speed and our Δt in the range 4–5 ms gives rather coarse acceleration estimates. New measurements with higher spatial and temporal resolution are required in order to accurately capture the accelerations in the regions with the strong velocities and velocity gradients.

We finally note that the experimental laboratory waves reported here have stronger nonlinearity (ϵ in the range 0.40–0.46) than the Camille and Draupner waves where the value of ϵ is 0.38–0.39 using the definition in Eq. (1).

Acknowledgements

The authors are grateful for the available funds and the possibility to present a preliminary version of this paper at the Workshop on Rogue Waves at the International Centre for Mathematical Sciences in Edinburgh 12–15 December 2005. This research was funded by the Research Council of Norway through the Strategic University Programme "Modelling of currents and waves for sea structures 2002-6" at the University of Oslo. The support is gratefully acknowledged.

References

[1] C.H. Kim, E. Randall, S.Y. Boo, M.J. Krafft, Kinematics of 2-D transient water waves using Laser Doppler Anemometry, J. Waterway, Port, Coastal Ocean Engrg. 118 (2) (1992) 147–165.

[2] T.E. Baldock, C. Swan, P.H. Taylor, A laboratory study of nonlinear surface waves on water, Philos. Trans. Roy. Soc. London A 354 (1996) 649–676.

[3] D. Skyner, A comparison of numerical predictions and experimental measurements of the internal kinematics of a deep-water plunging wave, J. Fluid Mech. 315 (1996) 51–64.
[4] J. Grue, D. Clamond, M. Huseby, A. Jensen, Kinematics of extreme water waves, Appl. Ocean Res. 25 (2003) 355–366.
[5] M. Perlin, J.-H. He, L.P. Bernal, An experimental study of deep water plunging breakers, Phys. Fluids 8 (1996) 2365–2374.
[6] M.Y. Su, Three-dimensional deep water-waves. Part 1. Experimental measurements of skew and symmetric wave patterns, J. Fluid Mech. 124 (1982) 73–108.
[7] A. Jensen, J.K. Sveen, J. Grue, J.-B. Richon, C. Gray, Accelerations in water waves by extended particle image velocimetry, Exp. Fluids 30 (2001) 500–510.
[8] A. Jensen, G.K. Pedersen, Optimization of acceleration measurements using PIV, Meas. Sci. Technol. 15 (2004) 2275–2283.
[9] A. Jensen, G.K. Pedersen, D.J. Wood, An experimental study of wave run-up at a steep beach, J. Fluid Mech. 486 (2003) 161–188.
[10] D. Clamond, J. Grue, Interaction between envelope solitons as a model for freak wave formations, C. R. Mecanique 330 (2002) 575–580.
[11] K. Trulsen, Wave kinematics computed with the nonlinear Schrödinger method for deep water, Trans. ASME 121 (1999) 126–130.
[12] D.A.G. Walker, P.H. Taylor, R. Eatock Taylor, The shape of large surface waves on the open sea and the Draupner New Year wave, Appl. Ocean Res. 26 (2004) 73–83.
[13] M.K. Ochi, Ocean Waves – The Stochastic Approach, Cambridge Univ. Press, Cambridge, 1998.
[14] K.-A. Chang, P.L.-F. Liu, Velocity, acceleration and vorticity under a breaking wave, Phys. Fluids 10 (1998) 327–329.
[15] A.L. New, P. McIver, D.H. Peregrine, Computations of overturning waves, J. Fluid Mech. 150 (1985) 233–251.
[16] D.G. Dommermuth, D.K.P. Yue, W.M. Lin, R.J. Rapp, E.S. Chan, W.K. Melville, Deep-water plunging breakers: a comparison between potential theory and experiments, J. Fluid Mech. 189 (1988) 432–442.
[17] G. Chen, C. Kharif, S. Zaleski, J. Li, Two-dimensional Navier–Stokes simulation of breaking waves, Phys. Fluids 11 (1) (1999) 121–133.